Solís-Casados *et al. J Mater. Sci: Mater Eng.* (2025) 20:62
https://doi.org/10.1186/s40712-025-00279-8

Journal of Materials Science: Materials in Engineering

ORIGINAL PAPER Open Access

Characterization of Pd-modified TiO_2-based thin films and their effect on photocatalytic activity

D. A. Solís-Casados[1], L. Escobar-Alarcón[2], R. López[3], D. S. García-Zaleta[4], J. M. Vázquez Rodríguez[4] and C. Encarnación-Gómez[4*]

Abstract

Thin film technology has made significant contributions to the field of photocatalysis through improvements in surface properties and a decrease in material costs. Therefore, the present study aims to evidence the properties that Pd can confer to TiO_2 thin films prepared by chemical vapor deposition technique and to verify their effectiveness as photocatalysts in the degradation reaction of the carbinol-based malachite green dye. TiO_2 films with different nominal Pd contents (2.8, 3.7, 4.6, and 6.4 at. % Pd) synthesized by CVD at 400 °C and 1 Torr pressure exhibit significant changes in their crystal structure, morphology, and electronic properties. On the one hand, at low concentrations (2.8 and 3.7 at. % Pd), substitutional doping is promoted. In contrast, the increase in concentration (4.6 and 6.4 at. % Pd) encourages the formation of PdO and $PdTiO_3$ phases, as indicated by X-ray diffraction, Raman spectroscopy, and X-ray photoelectron spectroscopy results. The anatase phase is partially inhibited by other phases, such as Pd–O and Ti-Pd–O; consequently, the grain size that constitutes the film is considerably reduced, and microstrains are increased. On the other hand, the study of the optical properties reveals a decrease in the bandgap energy and the recombination velocity of the charge carriers, resulting in a maximum degradation of 67% of the dye, which is obtained with film 4.6 at. % Pd, attributed to a synergistic effect between the observed properties.

Keywords TiO_2 thin films, Chemical vapor deposition, Photocatalytic degradation, Pd dopant

Introduction

The challenge of materials science is to find innovative solutions to improve the performance of photocatalytic, optoelectronic, and electrochromic devices, among others, for applications in the environmental (Gopinath et al. 2020), energy (Cruz et al. 2019), electronic (J. Liu et al. 2013), and chemical transformation areas (Jenck et al. 2004). In this sense, materials science can contribute to the development of new alternatives that overcome the drawbacks of extensively studied materials. Currently, environmental applications are a topic of constant study, and photocatalytic processes for wastewater remediation play a central role. Several organic and inorganic contaminants pose a serious threat to the health of the aquatic environment. Among the organic pollutants, cationic dyes, such as malachite green, are controversial

*Correspondence:
C. Encarnación-Gómez
cecilia.encarnacion@ujat.mx
[1] Centro Conjunto de Investigación en Química Sustentable UAEM-UNAM, Carretera Toluca-Atlacomulco, km. 14.5, Toluca, Estado de México C.P. 50200, México
[2] Departamento de Física, Instituto Nacional de Investigaciones Nucleares, Carr. México-Toluca S/N, La Marquesa Ocoyoacac, Estado de México 52750, México
[3] Tecnológico de Estudios Superiores de Jocotitlán (TESJo), Ejido de San Juan y San Agustín, Carretera Toluca-Atlacomulco km 44.8, Jocotitlán, Edo. México, México
[4] División Académica Multidisciplinaria de Jalpa de Méndez, Universidad Juárez Autónoma de Tabasco, Rancheria Ribera Alta, Tabasco, Carretera Estatal Libre Villahermosa-Comalcalco Km 27 S/N, Jalpa de Méndez C.P. 86205, México

due to their potential carcinogenic effects (Nandoost et al. 2022). Malachite green dye is a slightly basic, water-soluble compound. It is widely used as a dye in the textile, aquaculture,and food industries (Sharma et al. 2023). However, it has been previously reported that the malachite green molecule exhibits high persistence and bioaccumulation in aquatic organisms, which, as part of the food chain, are eventually consumed by humans and may lead to effects such as carcinogenesis, teratogenesis, and mutagenesis (Lellis et al. 2019). Therefore, addressing malachite green dye in wastewater is crucial to prevent harm to both animals and humans. Among the most studied photocatalytic materials for the degradation of organic dyes, TiO_2 is a semiconductor that presents essential advantages that have been widely reported but at the same time presents limitations such as the energy required for its photoactivation and the rapid recombination of charge carriers that generate reactive species necessary in photodegradation reactions (Dong et al. 2015). Additionally, TiO_2 powders are challenging to recover from wastewater systems (Sarma et al. 2023). Therefore, many options are being studied to enhance the photocatalytic response of TiO_2. Notably, the incorporation of metal ions into the titania crystal lattice can significantly extend the absorption of TiO_2 into the visible region (Rahman et al. 2023). In this way, the photocatalytic activity of TiO_2 is substantially dependent on the nature of the dopant ion, the dopant concentration, and the preparation method. On the one hand, the material used as dopant includes transition metals (Ni, Pt, Co, Nb, Pd) (Duta et al. 2016; Ganesh et al. 2012; Pan et al. 2018), metalloids (B, Si, Ge) (Cano-Casanova et al. 2022), and non-metals (C, N, P, F, Cl) (Camps et al. 2010; Irie et al. 2003), which have been utilized to modify the photocatalytic behavior by the visible light absorption of the TiO_2. Pd can be used as a dopant for various materials, such as $InVO_4$-TiO_2, where an increase in the photocatalytic activity of thin films for the decomposition of methyl orange dye has been observed. According to this study, Pd can act as an electron trap, facilitating electron–hole separation and subsequent transfer of the trapped electron to the surface of $InVO_4$-TiO_2 oxides (Ge & Xu 2006). Pd doping can also increase the visible light absorption capacity of metal oxides such as CeO_2. In this case, 1–5% Pd-doped CeO_2 has shifted the absorption edge to the visible region and decreased the recombination of electron–hole pairs (Matussin et al., 2023). Among other materials with photocatalytic efficiency, perovskite-type materials exhibit promising properties for various chemical reactions due to their high electronic mobility, high absorption coefficients, and longer charge carrier lifetimes (Dandia et al. 2020). For this reason, perovskite-type materials have been evaluated in photocatalytic water-splitting reactions (W. Wang et al. 2020), dye photodegradation (Gade et al. 2018), and methanol oxidation (Meng et al. 2022). However, despite the similarity between the ionic radii of Ti^{4+} (0.61 A) and Pd^{2+} (0.64 nm), the partial substitution of Ti^{4+} by Pd^{2+} to form the $PdTiO_3$ compound has not been reported. The addition of other cations to TiO_2 to increase its photocatalytic efficiency has been studied in perovskites such as $ZnTiO_3$, $BaTiO_3$ (Panthi & Park 2022), $SrTiO_3$ (Sohrabian et al. 2023), and $CaTiO_3$ (Passi & Pal 2021), where the addition of the cation favors the separation of the photogenerated carriers and provides optimal active sites for different chemical reactions. Instead, perovskite-type systems have been reported involving the exchange of the Pb^{2+} ion for Pd^{4+} in the $PbTiO_3$ compound, which serves as a multiferroic material, or the incorporation of the Pd^{4+} ion into $LaFeO_3$, resulting in the formation of $LaFe_{0.97}Pd_{0.03}O_3$ (Eyssler et al. 2010).

Apart from that, the method used to obtain photocatalysts, as in the case of thin films, is strongly influenced by the chemical, structural, morphological, and optical properties (Acosta-Silva et al. 2024; Nath et al. 2023). Various methods, including those in the vapor or liquid phase, have been used to prepare thin films. The most common thin film synthesis methods include sol–gel/spin coating, chemical precipitation, sputtering, spray pyrolysis, laser ablation, and chemical vapor deposition (CVD) (Chaudhari 2021; Kumar Patnaik & Divya 2023; Toma et al., 2024).

In particular, the metal–organic chemical vapor deposition process (MOCVD) offers several significant advantages, including a high deposition rate, improved control over film thickness, uniformity in thin films on substrates with complex geometric shapes, and adequate film adhesion to the substrate. CVD applications involve applying solid thin-film coatings to surfaces, which are also used to produce high-purity bulk materials and powders, as well as to fabricate composite materials. They have also been used to deposit an extensive range of materials. Accordingly, this proposal presents the synthesis of Pd-doped TiO_2 thin films using the chemical vapor deposition (CVD) technique, along with their chemical, structural, morphological, and photocatalytic performance in malachite green degradation. Although Pd is a relatively expensive metal, the use of thin films allows its use to be reduced while taking advantage of its unique properties. Similarly, using thin films as photocatalysts facilitates their removal from reaction systems, thereby representing a convenient advantage.

Experimental/methodology

TiO_2 and Pd-doped TiO_2 thin films were prepared in a horizontal hot-walled CVD reactor, supported on 4 cm^2

amorphous glass substrates that had been previously cleaned in an ultrasonic bath with an acetone–water solution and then air-dried. The precursors used were titanium isopropoxide ($Ti[OCH(CH_3)_2]_4$, Aldrich, 98%) and palladium acetylacetonate ($[CH_3COCH=C(O\text{-})CH_3]_2Pd$, Aldrich, 99%). Both precursors were mixed and frozen to evaporate inside the reactor and conducted by the carrier gas (argon) to the deposition zone. TiO_2 thin films were obtained under the following deposition conditions: Ar flow rate, 100 cm^3 min; deposition temperature,400 °C; total system pressure, 1 Torr; decomposition temperature of the precursors,120 °C; and deposition time, 20 min. The nominal Pd contents for TiO_2 doping were 2.8, 3.7, 4.6, and 6.4 at. %. The samples were labeled according to their nominal Pd contents, and the undoped sample was designated as undoped TiO_2. Figure 1 shows a schematic representation of the reaction system used for the deposition of TiO_2 and doped TiO_2 films. TiO_2 films obtained directly from the CVD reactor synthesis were characterized and evaluated in the photocatalytic degradation reaction without any additional post-treatment.

The chemical, structural, morphological, and optical properties of TiO_2 thin films were investigated using X-ray diffraction(XRD), Raman spectroscopy, Fourier transformed infrared spectroscopy (FT-IR),X-ray photoelectron spectroscopy (XPS), scanning electron microscopy (SEM), UV–Vis spectroscopy, and photoluminescence spectroscopy.

A Bruker D8 advanced diffractometer with Cu Kα radiation was used to identify the phases and determine the crystalline structure and microstrain of the thin films. Measurements were performed in the 2θ range from 20° to 90° with a step of 0.02°. The crystal size of the films obtained by CVD was determined from the diffraction patterns and the Scherrer equation (Eq. 1).

$$D = \frac{0.9\lambda}{\beta cos\theta} \tag{1}$$

where θ is the Bragg diffraction angle, λ is the wavelength of the X-ray radiation(1.5406 Å), and β is the full width at half maximum (FWHM) of the diffraction. FWHM was determined by fitting the XRD peaks to a non-linear Gaussian curve using ORIGIN software. On the other hand, other important parameters, such as micro-deformations in the crystal lattice, were determined by X-ray diffractograms to evaluate the effect of the dopant on the structural properties of the TiO_2 film. Microstrain (ε) is a measure of the degree of distortion induced in this case by the addition of a dopant (Eq. 2). ε is a function of FWHM (β) and Bragg angle θ.

$$\varepsilon = \frac{\beta}{4\tan\theta} \tag{2}$$

Raman spectra of the samples were recorded using a PerkinElmer spectrophotometer model Spectrum GX in the spectral range of 100–900 $cm^{-1}$with a 1064 nm laser. The elemental chemical composition of the thin films was determined by XPS using a JEOL JPS- 9200 with an Mg Kα X-ray source (1253.6 eV).FT-IR results were obtainedusing an Infrared Spectrum Two spectrophotometer (PerkinElmer, Waltham, MA, USA) in the spectral region from 450 to 2500 cm^{-1}. The surface morphology of undoped TiO_2 and TiO_2-Pd thin films was observed using a JEOL-6300 scanning electron microscope at an accelerating voltage of 20 kV. The recombination rate of the photogenerated charge carriers was determined using the photoluminescence spectroscopy technique (PL). Photoluminescence

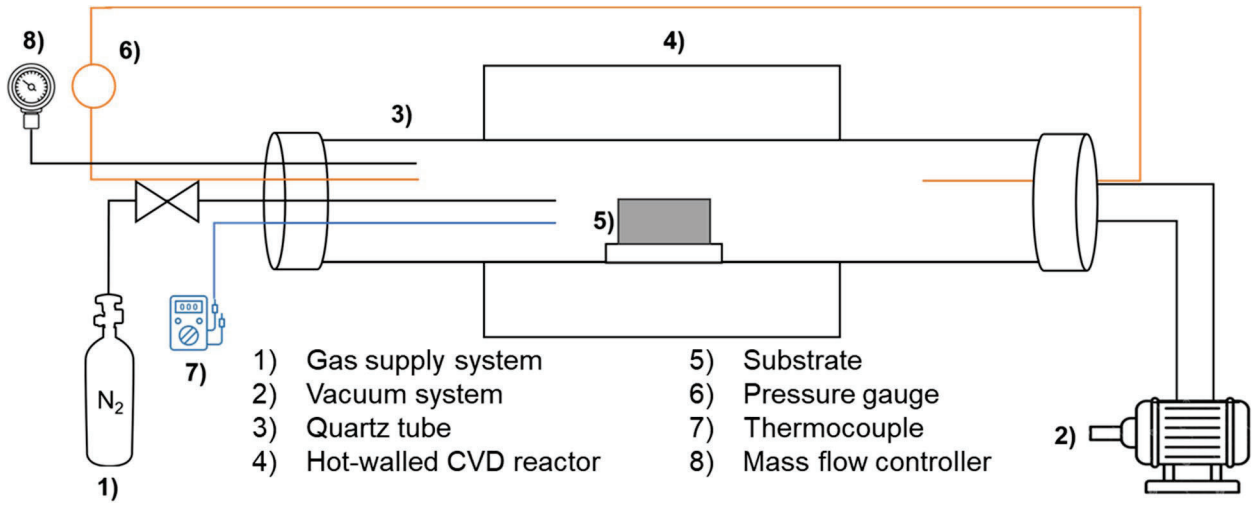

Fig. 1 CVD reactor scheme for the deposition of undoped TiO_2 and TiO_2-Pd thin films

spectra were recorded on a Cary Eclipse Agilent spectrophotometer equipped with a thermostated cell holder and Xenon Flash Lamp. The emission spectra were obtained with an excitation source fixed at 380 nm, corresponding to the maximum absorbance in the UV–Vis spectra. Additionally, a wavelength of 280 nm was used to determine the bandgap energy of the undoped TiO_2 and doped films. The optical properties of TiO_2 films were estimated from the UV–Vis spectra recorded on a PerkinElmer Lambda 35 spectrophotometer. Bandgap energy was also obtained from UV–Vis spectra using the Tauc model derived from the Kubelka–Munk function. UV–vis spectra were also used to elucidate other properties of the films, such as their refractive index (h_f) and thickness *(t)*. To obtain the optical constants and the thickness of the thin films, the values of the maximum and minimum of the oscillations in the transmission range are taken. It is convenient to plot the T_M and T_m envelopes passing through the maxima (M) and minima (m) and to take the corresponding pair of values, as well as the value of the corresponding wavelength. The refractive index and thickness of the films are determined once these values are obtained. Equation 3 was used to determine the refractive index:

$$\eta_f = \left\{ \frac{-(n_0^2 + n_2^2)(1 - 2\rho_T) + \left[(n_0^2 + n_2^2)^2(1 - 2\rho_T)^2 - 4n_0^2 + n_2^2\right]^{1/2}}{2} \right\}^{1/2} \quad (3)$$

where η_f, η_0, η_1 is the refractive index of thin film, air (1.0), and amorphous glass substrate (1.5), respectively.$\rho_T = T_{max}/T_{min}$; T_{max} maxima transmittance and T_{min}minima transmittance.

Finally, the Goodman model was used to determine thickness through Eq. 4.

$$t = \frac{M_{ab}\lambda_a\lambda_b}{2(\lambda_a - \lambda_b)(n_f^2 - sin^2\theta_0)^{1/2}} \quad (4)$$

where n_f is the refractive index. λ_a y λ_b wavelengths of maximum and minimum transmittance, respectively. M_{ab} number of fringes separating these extrema. θ_0 is the angle of incidence of light (for normal incidence, $\theta = 0$).

The catalytic performance of the Pd doped TiO_2 thin films was studied by following the degradation of 25 ml of solution (10 mmol/L of malachite green MG, carbinol base), which was performed by monitoring the decrease in the characteristic absorption band of MG, by taking aliquots of 4 mL at different times through absorbance measurement (619 nm malachite green) and related with a concentration using the Lambert–Beer equation as a function of the irradiation time. All experiments were carried out at room temperature. Before the dye degradation reaction, the photocatalysts were placed in the malachite green solution without light irradiation for a stabilization time of 30 min. Additionally, the effect of simulated sunlight on the decomposition (photolysis) of malachite green molecules without a catalyst was investigated by measuring the change in concentration over time. The result is compared to the photocatalytic process using undoped TiO_2 and Pd-doped TiO_2films. The photocatalytic system is composed of a light source, emitting light via a solar simulator (Scientech SF150 model, class A), with an average intensity of 60 mW/cm^2. The distance between the light source and the reaction system was 15 cm. The reaction rate constant *(k)* was determined by considering a pseudo-first-order kinetic order (Eq. 5) from the reaction time versus ln [C] graph.

$$k = \frac{1}{t} Ln \frac{C_0}{C} \quad (5)$$

where C_0 is the initial concentration and C is the concentration at time t.

Results and discussion

X-ray diffraction

Figure 2 shows the X-ray diffraction (XRD) patterns of undoped TiO_2 and Pd-doped TiO_2 films with different nominal Pd dopant contents. The XRD pattern of undoped TiO_2 shows only characteristic reflections attributed to TiO_2 anatase phase (ICDD 21–1272) in 2θ of 25.44°, 48.14°, 55.20°, 70.47°, and 76.12°, corresponding to (101), (200), (211), (220), and (215) planes, respectively. At the deposition conditions of TiO_2 films described above, it becomes possible to obtain the crystalline arrangement associated with the anatase phase (Won et al. 2001). In the CVD process, at the deposition temperature of the films (400 °C), the formation of anatase polycrystalline is favored without heat after treatment. No other reflections related to different phases of TiO_2 were observed. When the Pd precursor is introduced into the reaction system, remarkable differences in the diffraction profile of the TiO_2 films can be observed. In Fig. 2B, a magnification of the (101) reflection is observed, which shows a slight shift of this peak with the addition of Pd.is On the one hand, it is possible to appreciate a slight change in 2θ of the (101) plane when the nominal Pd content is 2.8 and 3.7 at.% Pd (Fig. 2B and Table 1). It is essential to note the significant increase in the FWHM (full width at half maximum) when the maximum concentration of Pd, as studied in this work, is reached. In addition to the rise in FWHM, the decrease in crystal size with increasing Pd concentration suggests that there is an

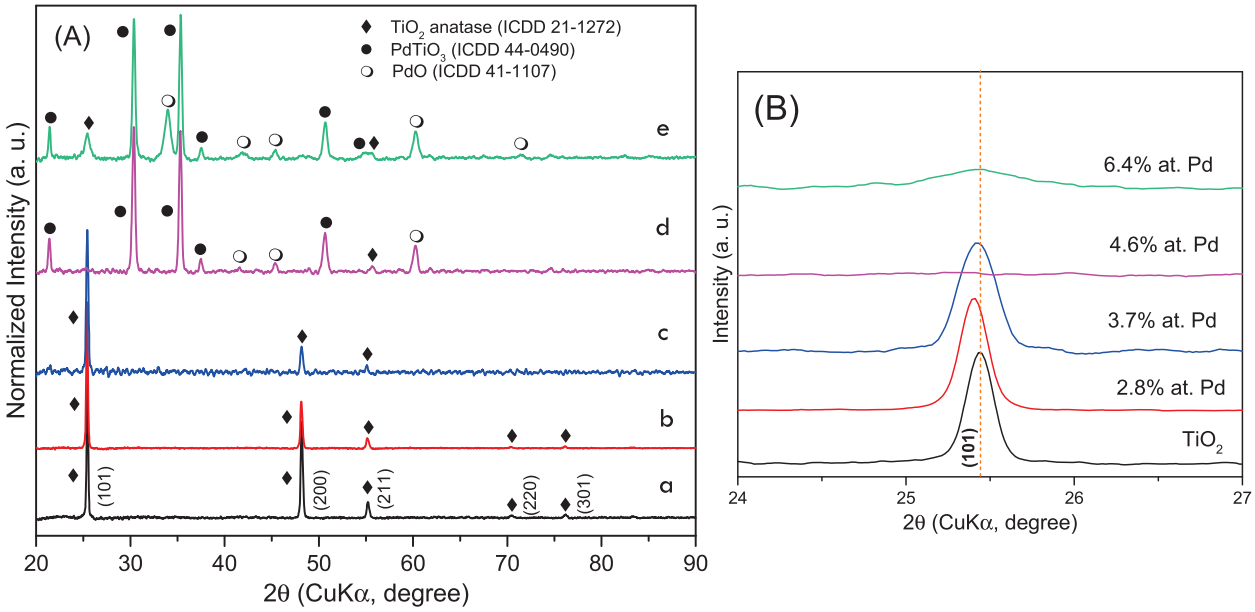

Fig. 2 **A** X-ray diffraction patterns of TiO_2-Pd films with different nominal Pd content; a. Undoped TiO_2 film; b. 2.8 at. % Pd; c. 3.7 at. % Pd; d. 4.6 at. % Pd; e. 6.4 at. % Pd. **B** Amplification of (101) reflection

Table 1 XRD parameters for TiO_2 films obtained by (101) reflection

Film	2q (degrees)	FWHM (degrees) [full width at half maximum]	Crystal size (nm)	Microstrain ($\times 10^{-3}$)
TiO_2	25.44	0.19	43.3	3.79
2.8 at. % Pd	25.40	0.20	42.1	3.91
3.7 at. % Pd	25.42	0.26	32.0	5.14
4.6 at. % Pd	–	–	–	–
6.4 at. % Pd	25.43	0.69	12.3	13.3

integration of the dopant into the TiO_2 structure, which limits the crystallization of the anatase phase and eventually leads to the formation of $PdTiO_3$ crystals (ICCD 44–0490) and PdO (ICCD 41–1107).Therefore, the films with 4.6 and 6.4 at. % Pd are constituted by a mixture of TiO_2 anatase, $PdTiO_3$ and PdO phases.

An increase in microstrain is expected due to the presence of the phases described between Ti, Pd, and O (Table 1). Some authors have reported that the metal-doping of TiO_2 influences the crystallization of TiO_2 (Lu et al. 2016; Mekprasart et al. 2013).

Raman spectroscopy

Raman spectroscopy was employed to elucidate the crystalline structure of TiO_2 films and validate the XRD results. Figure 2a shows the Raman spectra of undoped TiO_2 and Pd-doped TiO_2 films. The Raman lines at 142.07, 196.4, 396.31, 515.12, and 639.26 cm^{-1} can be assigned to the $E_g(1)$, Eg(2), B1 g, A1 g, and Eg(3) vibration modes, respectively. These vibration modes are attributed to the TiO_2 anatase phase in agreement with XRD results. The inclusion of Pd dopant in TiO_2 films results in a shift of the peak position to the higher energy side and a broadening of the full width at half maximum (FWHM) of the anatase main mode [E_g (1)] [see Fig. 3b and Table 2]. Like another metal dopant previously reported, the Pd dopant may cause deformation in the TiO_2 structure, and stabilization of the structure is achieved through the formation of Ti–O–Pd or Pd–O–Pd bonds (B. Liu et al. 2009). Consequently, variations in the crystalline cell volume can be observed due to the differences in the ionic radius of the dopant and titanium, which affect the Raman-active modes. The ionic radius of Pd^{2+} (0.64 Å) is similar to that of Ti^{4+} (0.61 Å); thus, the lattice structure of TiO_2 could be slightly distorted, and the need to maintain neutral charge entails the formation of oxygen vacancies (Choudhury & Choudhury 2013). Some authors have attributed the TiO_2 lattice contraction to the presence of oxygen vacancies, as indicated by a Raman peak shift to a higher wavenumber (Zhang et al. 2015). These variations have been observed in the displacement of the characteristic vibration band of anatase using Ni, Co, Eu, Cu, and other metal dopants, indicating the incorporation of the dopant into the anatase lattice, occupying Ti sites (M. Pal et al., 2012). Nevertheless, given the similarity in ionic sizes of Pd^{2+} and

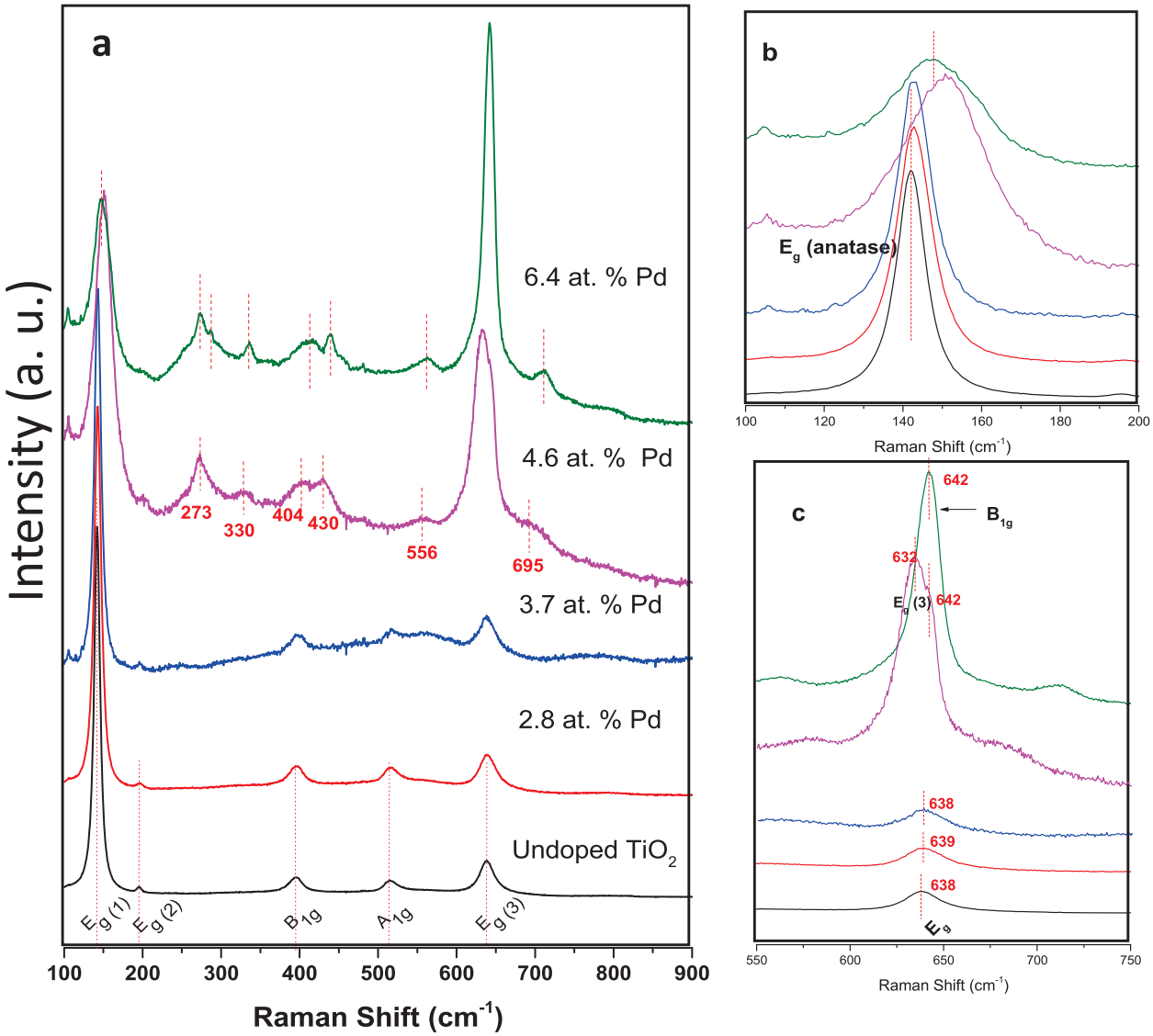

Fig. 3 **a** Raman spectra of undoped TiO_2 and Pd-doped TiO_2 films. **b** E_g (1) mode displacement. **c** E_g (3) and B_{1g} modes overlapping

Table 2 Variation of E_g (1) mode and FWHM with Pd content

Film	Position [E_g (1) mode-cm^{-1}]	FWHM (cm^{-1})
Undoped TiO_2	142.035	11.077
2.8 at. % Pd	142.828	12.877
3.7 at. % Pd	142.871	11.790
4.6 at. % Pd	152.018	32.281
6.4 at. % Pd	147.712	27.184

Ti^{4+}, the replacement of Tiwith Pd in the TiO_2 structure islikely. Furthermore, other peaks can be observed at 642 cm^{-1}, which is very close to the E_g (3) mode of anatase (638 cm^{-1}) for 6.4 at. % Pd film (Fig. 3c). In the case of the 4.6 at. % Pd, these two vibration modes are partially overlapping and centered at 632 and 642 cm^{-1}. According to a study by J. R. McBride et al., the vibration modes at 642 and 439 cm^{-1} can be attributed to the B1 g and Eg-allowed Raman modes of PdO, with slight variations due to interaction with the TiO_2 anatase phase (McBride etal., 1991). The other minor features were observed in the Raman spectra, especially for 6.4 at. % Pd, at 336, 563, and 712 cm^{-1}, which could relate to the presence of $PdTiO_3$. This ABO_3 oxide type crystallizes in structures whose level of distortion and stability is mainly determined by the ratio of the ionic radius of the A y B cations. In this case, Pd^{2+}, Ti^{4+}, and

O^{2-} ions can be accommodated in an orthorhombic perovskite structure. For perovskite-type compounds, such as $BaTiO_3$—the most studied ferromagnetic perovskite—the bands around 310, 550, and 720 cm^{-1} correspond to the typical Raman peaks of $BaTiO_3$. The peak at 310 cm^{-1} is assigned to the B_1 mode and indicates the presence of the tetragonal phase. For its part, the bands around 550 and 720 cm^{-1} are assigned to the transverse optical (TO) modes of A1 symmetry and the highest-frequency longitudinal optical mode (LO) with A1 symmetry, respectively (Deng et al. 2010). Likewise, the ionic arrangement of Ti^{4+}, Pd^{2+}, and O^{2-} shares the same composition and structure as BaTiO3 perovskite; it is therefore possible to reasonably attribute the aforementioned vibration modes to $PdTiO_3$ perovskite.

The structural characterization carried out by XRD and Raman spectroscopy appears to indicate that Pd-doped films are composed of a phase combination of Pd partially replacing Ti, forming titanate-type compounds and palladium oxide (PdO) when the Pd dopant content exceeds 3.7 at. % Pd. It is possible that the Pd dopant at 2.8 and 3.7 at. % can replace Ti in substitutional sites or be incorporated into interstitial sites, as evidenced by the Raman displacement.

FTIR spectroscopy

The FTIR method is used to analyze surface films and investigate the impact of doping elements on the chemical properties of TiO_2. Figure 4 shows the IR spectra of TiO_2 undoped and TiO_2-doped films with different Pd loadings. The IR spectrum of undoped TiO_2 films on a glass substrate exhibits absorption bands at 836, 540, and 478 cm^{-1}, corresponding to vibrational modes attributed to the stretching vibration of Ti–O-Ti bonds in TiO_2. (Eleutério et al. 2020). In all spectra, a broader band centered around 1060 cm^{-1} is visible, corresponding to the Si–O-Si bonds of the amorphous glass substrate (Musić et al. 2011).

The original vibration modes observed in TiO_2 films exhibit an apparent decrease in intensity and a redshift of the band around 890 cm^{-1}, which can be attributed to the contribution of Pd to the TiO_2 crystal lattice. It is important to mention that no vibration bands attributed to Pd–O or Pd-TiO_3bonding, as in the case of other previously reported perovskites, are appreciated by this technique (Perdomo et al. 2008; Portia et al. 2020).

X-ray photoelectronic spectroscopy (XPS)

XPS determined the oxidation state of the species present in the TiO_2-based film surface. Figure 5a–c shows

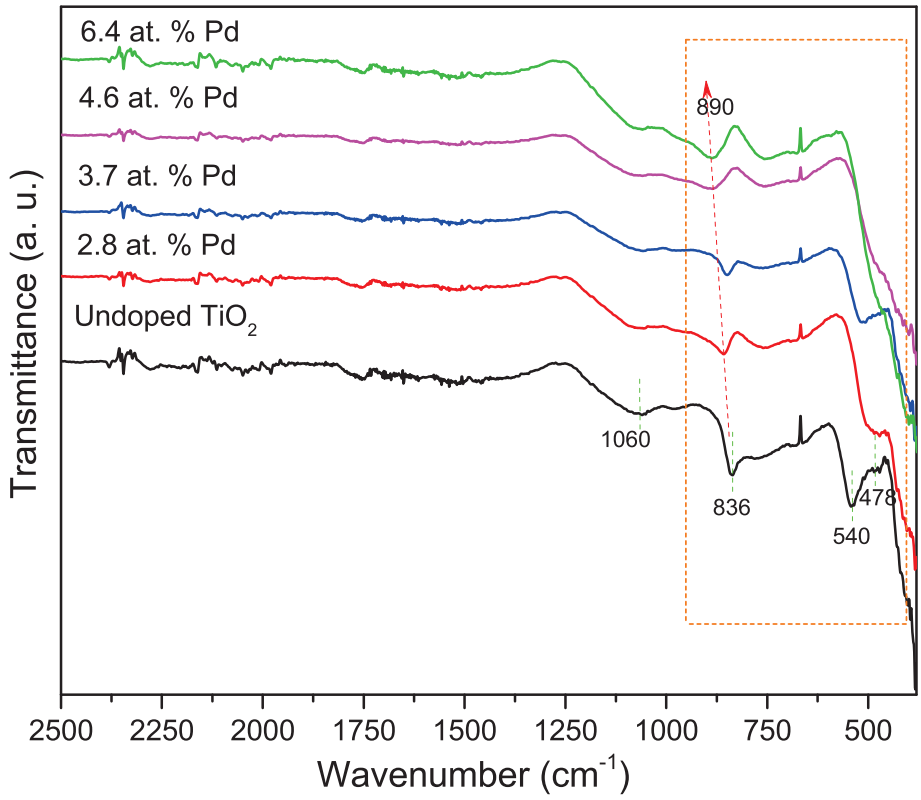

Fig. 4 FTIR spectra of undoped TiO_2 and Pd-TiO_2 films prepared by CVD

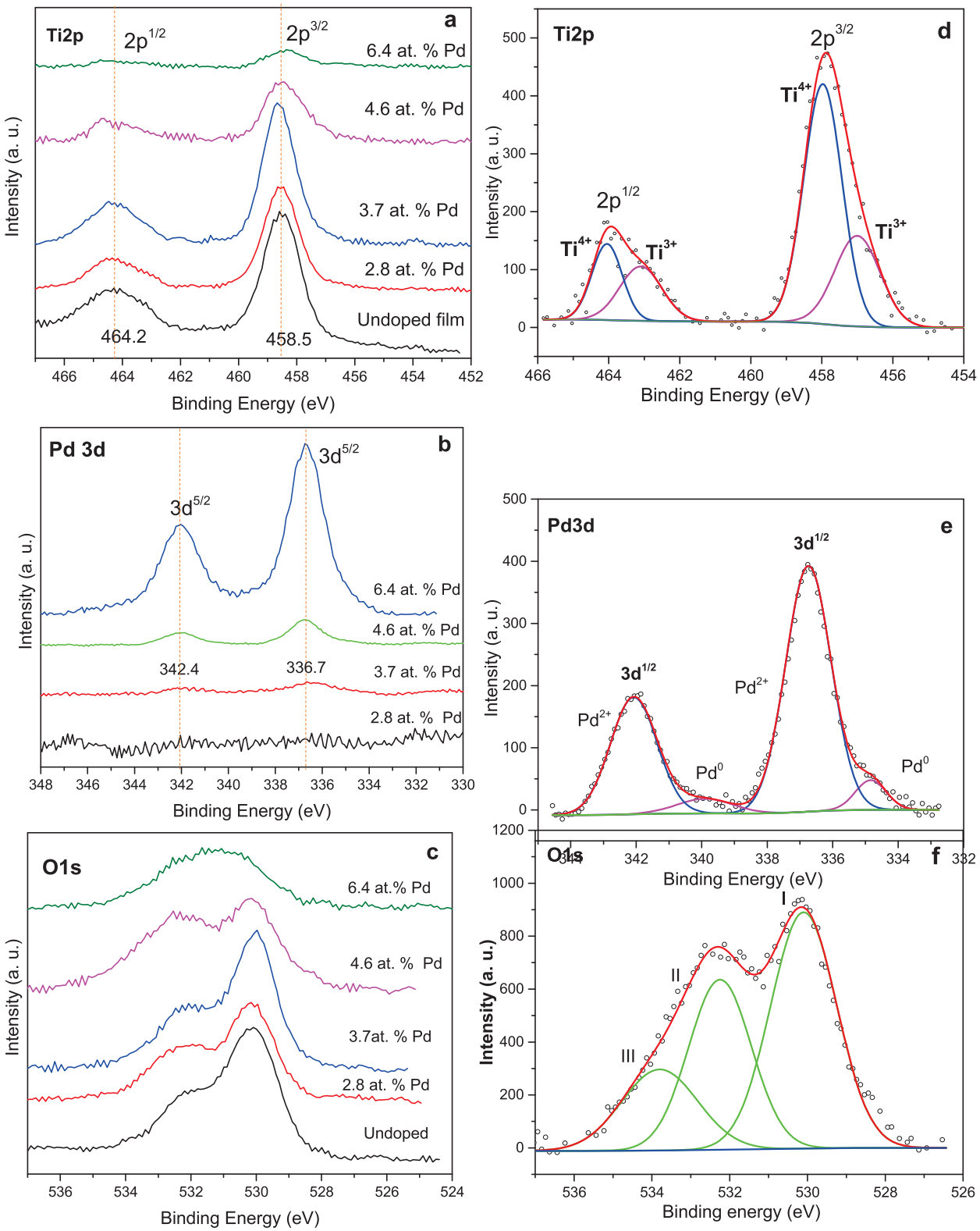

Fig. 5 XPS spectra of TiO_2-based thin films of regions: **a** Ti2p, **b** Pd3d **c** O1s, **d**, **e**, **f** Deconvoluted spectra of 4.6 at. % Pd in Ti2p, Pd3d, and O1s regions, respectively

the XPS spectra of TiO_2 films with different Pd contents, displaying the Ti2p, Pd 3 d, and O 1 s regions. For the undoped TiO2 film, the XPS spectra of Ti 2p present two spin–orbit components, 2p1/2 and 2p3/2, at 464.2 and 458.5 eV, corresponding to Ti^{4+} in a tetragonal structure of TiO_2 (Barreca et al. 2007). Pd dopant promotes notable changes in the chemical state of the films due to the formation of a new species, as evidenced by DRX and Raman spectroscopy. The dopant insertion into the TiO2 film results in a partial reduction of Ti^{4+} species to Ti^{3+}, as indicated by the deconvoluted peaks in the Ti2p region (Fig. 5d). The increased Ti^{3+} peak intensity may be related to the charge compensation by electrons for the substitutional doping of Pd^{2+} species for Ti^{4+} (Sathasivam et al. 2015). The electrons trapped in the vacancies interact with Ti^{4+} to reduce Ti^{3+}(Choudhury & Choudhury, 2012). Similarly, Fig. 5b, e shows the Pd3 d region with a double structure, each with two pairs of peaks. The first pair, at 336.7 and 342.4 eV, corresponds to Pd $3d^{5/2}$ and Pd $3d^{3/2}$, respectively. These contributions can be attributed to the presence of Pd^{2+} from Pd–O and Pd-Ti–O interactions. The other pair of peaks, at 334.2 and 339.2 (of low intensity), is attributed to Pd^0 (Feng et al. 2021). It should be noted that Pd^0 formation was only observed in films containing 4.6 and 6.4% at. Pd, possibly due to the synthesis conditions using Ar as a carrier gas, a proportion of the Pd precursor reacts with the TiO2 precursor, while another portion is reduced to Pd^0 at 400 °C. Finally, Fig. 5c, f present the O1 s signal, which is deconvoluted into three peaks with binding energies of approximately 530.1, 532.3, and 533.6 eV. The peak at 530.1 eV (peak I) is attributed to oxygen bonded in the perovskite-like structure. In comparison, the peak at 532.3 eV (peak II) is attributed to the oxygen vacancies generated by the substitution of Ti in the crystal lattice and the formation of Ti^{3+} species. Meanwhile, the peak at 533.6 eV (peak III) is attributed to oxygen atoms adsorbed on OH species, as reported in previous studies (Wu et al. 2015).

Scanning electron microscopy

SEM was used to study the morphological characteristics of the CVD-deposited TiO_2 thin films and the effect of Pd addition. Figure 6 shows the SEM images of

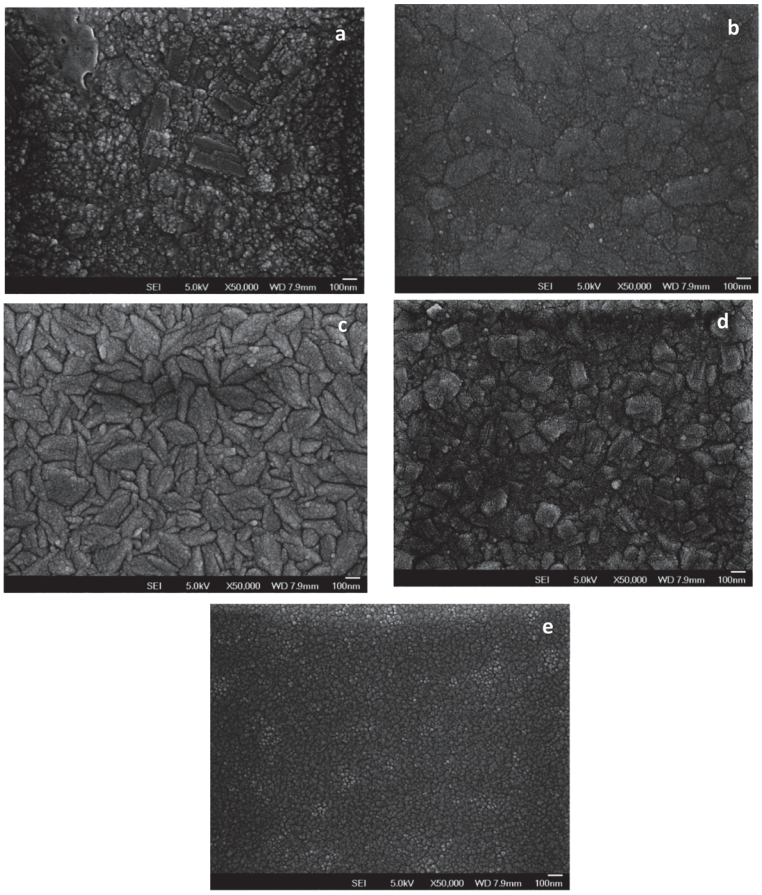

Fig. 6 SEM images of **an** undoped TiO_2; **b** 2.8 at. % Pd; **c** 3.7 at. % Pd; **d** 4.6 at.% Pd; **e** 6.4 at. % Pd

the TiO_2 thin films. Semi-spherical agglomerates, characteristic of nucleation and vapor-phase growth processes, comprise the surface morphology of the TiO_2 films. In this process, the precursor decomposes in the gas phase and is carried to a thermally activated substrate (at the deposition temperature), where heterogeneous reactions occur, forming the thin film.

The absence of well-defined grain boundaries indicates that there is no preferential growth direction, as they are deposited on amorphous substrates, and the arrangement tends to follow a compact growth pattern. Furthermore, Pd addition alters the surface morphology, and new grain boundaries are observed, defining regions formed by smaller particles with diameters below 100 nm. In the case of higher Pd content, these grain boundaries become less defined due to a significant decrease in the domains constituting the material. According to the XRD results, the inhibition of anatase crystallization leads to a reduction in crystal size; hence, the size of the particles consisting of crystals should consequently decrease, as observed in the Pd-doped TiO_2 films.

UV-Vis spectroscopy

Figure 7 shows the UV–Vis optical transmission spectra of undoped TiO_2 and Pd-doped TiO_2 films, analyzed at 300–1100 nm of wavelength. The TiO_2 spectrum is transparent in the visible range. It exhibits a wavy appearance due to light interference phenomena, while Pd incorporation causes a significant decrease in the optical transmission level at 6.4 at. % Pd from 80 to 50%. The reduction in transmittance of the films with the addition of Pd around 390 nm has been attributed to the excitation of electrons from the valence band to the conduction band.

This effect has been reported with dopant metals such as Pd and Ni (Kavi Rasu et al. 2020). In turn, the variation of the absorption edge of TiO_2 towards longer wavelengths is related to a decrease in the band gap energy. (Anis et al. 2019) On the other hand, this decrease in the transmittance level of the Pd-doped films is related to the UV–Vis radiation interaction of different phases, such as PdO and $PdTiO_3$ compared to TiO_2, as evidenced by XRD, as well as the increase in film thickness because of the increase in the metal content of the dopant. Figure 7b shows an inset corresponding to the Tauc graph from which the band gap energy was determined to be 3.2 eV for the TiO_2 anatase phase. The bandgap energy of the Pd-doped films is reported in Table 3. The refractive index values of the films show a significant change in the chemical properties with the addition of Pd. Similarly, the thickness of the films was determined by the refractive index. In general, the addition of the dopant increases the thickness of the films. This result is expected since

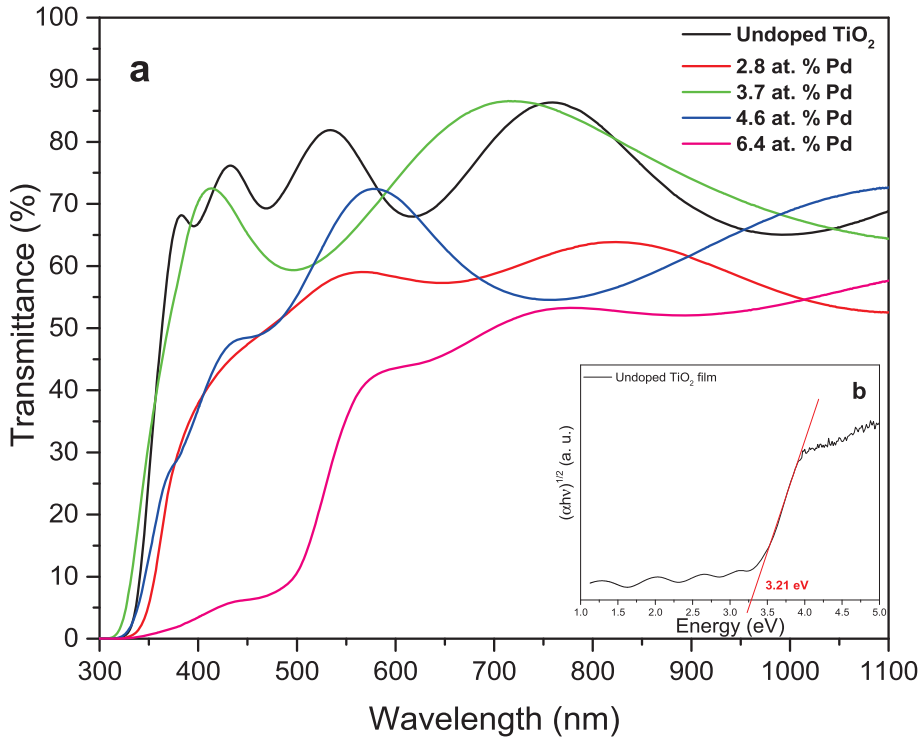

Fig. 7 **a** Transmittance spectra of undoped TiO_2 and Pd-doped TiO_2 films. **b** Bandgap energy of the undoped TiO_2 film

Table 3 Optical parameters of TiO_2 thin films

Film	Band gap energy (eV) [Tauc plot]	Band gap energy (eV) [PL spectra]	Refractive index	Film thickness (nm)
Undoped TiO_2	3.2	3.2	2.5	202
2.8 at. % Pd	3.0	2.9	2.9	237
3.7 at. % Pd	3.2	3.1	2.7	312
4.6 at. % Pd	3.1	2.9	3.4	345
6.4 at. % Pd	2.4	2.7	5.6	278

the precursor content must be increased to increase the dopant concentration in the film.

Photoluminescence spectroscopy

The optical excitation of a semiconductor and the subsequent emission of radiation by this system are collectively referred to as photoluminescence (PL). This process occurs when a semiconductor is excited by electromagnetic radiation with an energy quantum greater than its band gap, resulting in the generation of an electron–hole pair (Liqiang et al. 2006). Therefore, the PL technique is used to evaluate the recombination rate of charge carriers and relate it to the photocatalytic activity of semiconductor materials. Figure 8 shows the photoluminescence (PL) spectra of TiO_2-doped and undoped films obtained using wavelength excitation at 380 nm. The spectrum of the undoped film obtained using an excitation wavelength of 280 nm is included as an insert in Fig. 8. The inset shows the characteristic band gap energy of TiO_2 at 3.23 eV.

The excitation peaks of the undoped TiO_2 films are located at approximately 457, 459, 485, 519, 541, 475, and 586 nm. Meanwhile, the PL spectra of thePd-doped films exhibit peaks at similar wavelengths to those of the undoped TiO_2 film. These visible emission peaks have been attributed to electrons trapped in the oxygen vacancies and defects of semiconductors (Gandhi & Wu 2017). However, the addition of Pd causes a significant decrease in the PL intensity. It has been reported that the incorporated metal dopant acts as an electron trap, suppressing the electron–hole pair recombination process and thereby increasing catalytic activity due to a more significant number of available reactive species (Abdullah et al. 2017). In this sense, the decrease in photoluminescent intensity with the increase in the amount of Pd added can be attributed to the fact that there is a slower rate of recombination of electron–hole pairs, and consequently, fewer electrons will return to the conduction band, emitting less energy in the form of light (Daude et al. 1977; Kavi Rasu et al. 2020). Although the decrease in PL intensity is not proportional to the increase in dopant concentration in the films, it can be generally observed that there is an apparent decrease in the carrier

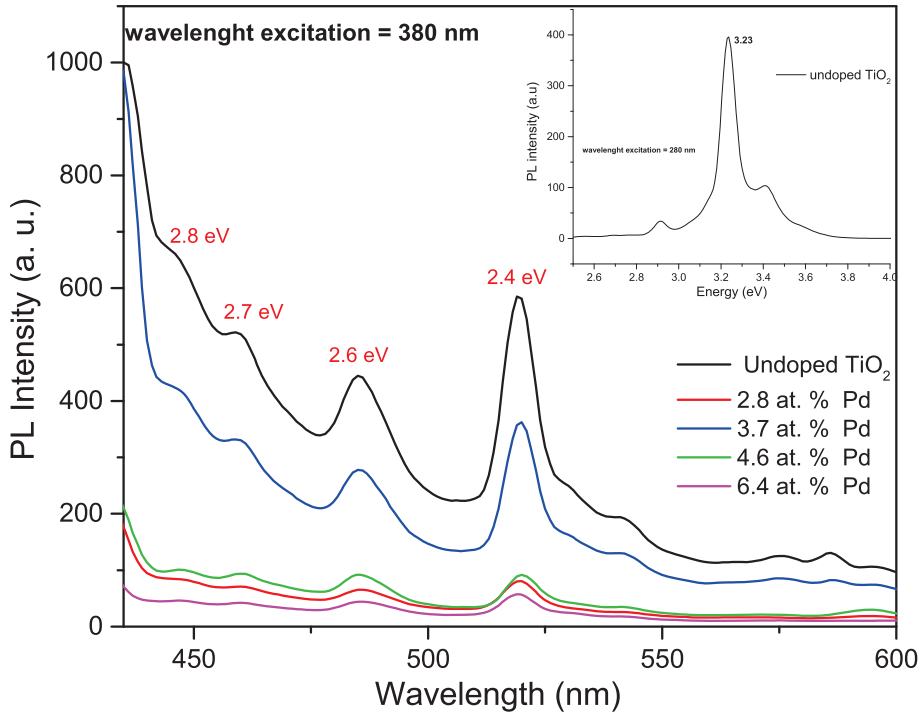

Fig. 8 Photoluminescence spectra of undoped TiO2 and Pd-doped TiO2 films. The inset corresponds to the bandgap energy of the undoped TiO_2 film, as determined by photoluminescence (PL)

recombination rate with the addition of Pd, which could have a positive effect on the photocatalytic performance of the films. Table 3 presents the bandgap energy of the analyzed films, as determined by photoluminescence (PL) spectra. Compared to the bandgap energy determined by UV–Vis spectroscopy, both exhibit a decrease with the addition of Pd with slight variations due to the technique used. It is important to note that a decrease in crystal size is associated with a decrease in photoluminescent intensity (Metéis & Singh, 2014), resulting in higher catalytic activity compared to the TiO_2 film.

Table 4 Parameters of the photocatalytic evaluation in the degradation reaction of MG dye

Film	Band gap energy (eV)	Rate constant $k \times 10^{-4}$ (min^{-1})[a]	Degradation (%)[a]
Photolysis	–	8.56	14.1
TiO_2	3.2	24.64	34.7
2.8 at. % Pd	2.9	33.84	44.0
3.7 at. % Pd	3.1	44.40	56.0
4.6 at. % Pd	3.0	62.35	67.0
6.4 at. % Pd	2.9	42.75	53.0

[a] At 180 min of reaction

Photocatalytic activity

The photocatalytic evaluation of the TiO_2-based films was carried out by monitoring the degradation reaction of the carbinol-based malachite green dye under simulated sunlight. Figure 9 shows the C/C_0 vs. reaction time graph in which an evident decrease in the concentration of the dye in the systems catalyzed by the thin films can be seen. Table 4 shows the key parameters related to photocatalytic activity.

It is worth noting that the highest degradation was observed at 4.6 at. % Pd film (67%), with its corresponding highest reaction rate constant of 62.35 $\times 10^{-4}$ min^{-1}, compared to the other films evaluated. The photocatalytic activity of these films is related to several factors, as evidenced by the study of their structural, morphological, and optical properties, which were previously determined. Firstly, the doping of the TiO_2 crystal structure at contents of 2.8 and 3.7 at. % Pd and the reduction of the crystal size, which could allow a stronger interaction with the dye. Additionally, the well-known effect of doping on decreasing the bandgap energy and the recombination rate of charge carriers is also evident. Secondly, the photoactivity observed in the film with 4.6 at. % Pd appears to be related to the incipient formation of combined Pd–O and Pd-Ti–O phases. Specifically, although there are few reports, the formation of perovskite with Pd is possible due to the metastable conditions generated in the CVD reactor. According to XRD results, the transformation to the orthorhombic phase, as reported in ICDD chart 44–0489, can be achieved by partially substituting Ti^{4+} ions with Pd^{2+} ions. The increase in Pd content leads to the formation of PdO, which also, according to previous studies, may have some effect on the electronic structure of the base semiconductor and have an impact on the decrease of the recombination rate of electron–hole

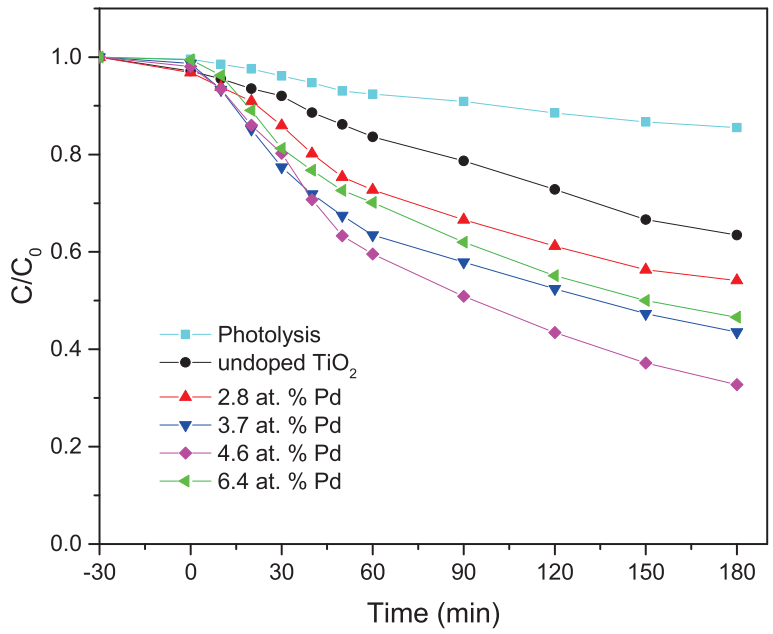

Fig. 9 Photocatalytic activity of TiO_2-based films in the degradation of the MG dye

pairs, which ultimately impacts on a higher photocatalytic efficiency (Ismail 2012; R. Wang et al. 2021). In addition, the presence of Pd^0 in the films with 4.6 and 6.4 at. % Pd, as determined by XPS, may influence photocatalytic activity. In principle, it has been reported that Pd^0 is catalytically active. Thus, the presence of Pd in the reduced state may favor enhanced photodegradation under visible light irradiation (Yu et al. 2015).

Figure 10 shows a plausible reaction mechanism for the degradation of malachite green dye by Pd-doped TiO_2 thin films. The absorption of visible-wavelength photons causes the photocatalytic reaction on the surface of a Pd-doped TiO_2 film, leading to the degradation of MG dye. The electron/hole pair photogenerated by simulated sunlight irradiation is mediated by the presence of the photocatalyst. The addition of Pd modifies the bandgap energy and affects the trapping and recombination of the generated electrons and holes, thus decreasing the recombination rate of the electron/hole pair. The chemical species present on the film surface favor the formation of O_2^{*-} and HO* radicals, which oxidize the dye and reduce it to smaller organic fragments that are finally mineralized to CO_2 and H_2O (Eq. 6-10).

The decomposition mechanism of the MG dye is described as follows (Eqs. 6-10):

$$TiO_2 - Pd + h\nu \rightarrow TiO_2 - \left(e^- + h^+\right) \quad (6)$$

$$TiO_2 - Pd\left(e^-\right) + O_2 \rightarrow TiO_2 - Pd\left(O_2^{*-}\right) \quad (7)$$

$$MG_{dye} + O_2^{*-} \rightarrow MG_{dye}\left(\text{fragments}\right) \rightarrow CO_2 + H_2O \quad (8)$$

$$TiO_2 - Pd\left(h^+\right) + H_2O \rightarrow TiO_2 - Pd\left(OH^*\right) + H^+ \quad (9)$$

$$Mg_{dye} + OH^* \rightarrow MG_{dye} \rightarrow CO_2 + H_2O \quad (10)$$

Conclusions

Pd-doped TiO_2 films with low Pd concentrations (2.8 and 3.7 at. % Pd) exhibit effective doping of the TiO_2 structure, as evidenced by XRD, Raman, FTIR, and XPS. This structural modification of TiO_2 results in a decrease in crystal size and an increase in microdeformation due to the presence of Pd, as it partially inhibits the crystallization of anatase. The known effect of the addition of the dopant was observed in the slight decrease in the bandgap energy of TiO_2 with the incorporation of Pd, as well as the consequent reduction in PL intensity related to the inhibition of the recombination process of the e^-/h^+ pair, or else, to the formation of oxygen vacancies and other surface defects. Although photocatalytic efficiency is a multifactorial phenomenon, in the present study, it can be observed that in films with lower dopant concentrations, the decrease in grain size, as determined by SEM, dominates. This is because the formation of well-defined and smaller grain boundaries generates zones of higher reactivity within the film. Additionally, the decrease in crystal size is associated with a reduction of photoluminescent intensity. On the other hand, an increase in dopant concentration is not necessarily reflected in an increase in photoactivity. Specifically, the 4.6 at. The Pd film presents the highest photocatalytic activity, mainly attributed to the presence of Pd^0, Pd^{2+}, Ti^{3+}, and Ti^{4+} species that can contribute to the formation of OH^* and O_2^{*-} radicals or generate intermediate levels in the energy band of TiO_2. In the $PdTiO_3$ compound specifically, Ti^{4+} is replaced by Pd^{2+}, and the generation of oxygen vacancies is necessary to compensate for this charge imbalance. The role of photocatalytic activity played by surfaces containing Ti^{3+} ions is significant due to exhibiting good absorption of visible light. Finally, it can be said that the photocatalytic activity observed in Pd-doped TiO_2 films is strongly linked to

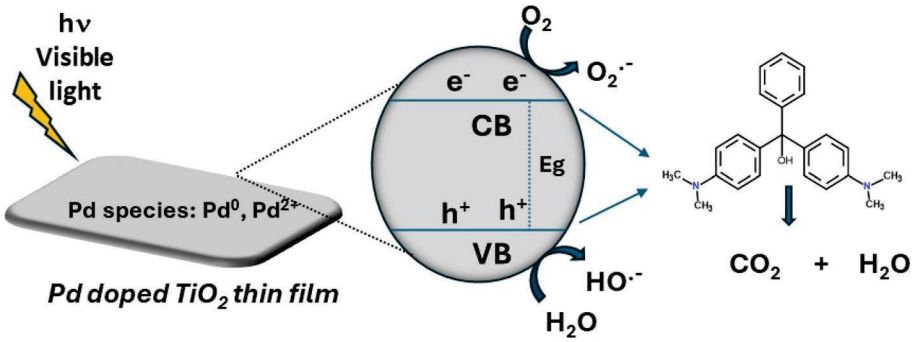

Fig. 10 Proposed reaction mechanism for the degradation of malachite green dye by Pd-doped TiO_2 thin films

the compounds formed during the vapor phase synthesis process and the balance between the higher or lower activity attributed to the species formed, as well as to the physical and optical properties of the film, is a topic of interest to be studied, since the photoactivity of $PdTiO_3$ which has not been previously explored is being reported.

Authors' contributions

Conceptualization: C. Encarnación-Gómez and D. A. Solís-Casados. Data curation: C. Encarnación-Gómez and D. S. García Zaleta. Formal analysis: D. A. Solís-Casados and C. Encarnación-Gómez. Investigation and methodology: R. López and D. S. García-Zaleta. Resources: D. A. Solís-Casados and J. M. Vázquez-Rodríguez. Supervision: D. A. Solís-Casados and L. Escobar-Alarcón. Writing: C. Encarnación-Gómez. Writing—review and editing: R. López and J. M. Vázquez-Rodríguez.

Funding

C. Encarnación thank CONAHCYT for the support provided through the program "Estancias Posdoctorales Nacionales para el fortalecimiento del Posgrado".

Data availability

The datasets used and/or analyzed during the current study are available from the corresponding author on reasonable request.

Declarations

Competing interests

The authors declare that they have no competing interests.

Received: 26 November 2024 Accepted: 14 April 2025
Published online: 30 April 2025

References

Abdullah H, Khan MMR, Ong HR, Yaakob Z (2017) Modified TiO2 photocatalyst for CO2 photocatalytic reduction: An overview. J CO2 Utilization 22:15–32. https://doi.org/10.1016/J.JCOU.2017.08.004

Acosta-Silva YD, Gallardo-Hernández S, Rivas S, Espejel-Ayala F, Méndez-López A (2024) Photocatalytic Activities of Methylene Blue Using ZrO2 Thin Films at Different Annealing Temperatures. Coatings 14(5):537. https://doi.org/10.3390/coatings14050537

Anis M, Muley GG, Baig MI, Rabbani G, Ghramh HA, Ramteke SP (2019) Doping effect of Ni2+ on structural, UV-visible, SHG efficiency, dielectric and microhardness traits of KH2PO4 (KDP) crystal. Optik 178:752–757. https://doi.org/10.1016/j.ijleo.2018.10.061

Barreca D, Gasparotto A, Maccato C, Maragno C, Tondello E (2007) TiO2 Thin Films by Chemical Vapor Deposition: An XPS Characterization. Surf Sci Spectra 14(1):27–33. https://doi.org/10.1116/11.20070902

Camps E, Escobar-Alarcón L, Camacho-López MA, Solís-Casados DA (2010) Visible-light photocatalytic activity of nitrided TiO2thin films. Mater Sci Eng, B 174(1–3):80–83. https://doi.org/10.1016/j.mseb.2010.03.020

Cano-Casanova L, Ansón-Casaos A, Hernández-Ferrer J, Benito AM, Maser WK, Garro N, Lillo-Ródenas MA, Román-Martínez MC (2022) Surface-Enriched Boron-Doped TiO2Nanoparticles as Photocatalysts for Propene Oxidation. ACS Appl Nano Mater 5(9):12527–12539. https://doi.org/10.1021/acsanm.2c02217

Chaudhari MN (2021) Thin film deposition methods: A critical review. Int J Res Appl Scie Eng Technol 9:5215–5232. https://doi.org/10.22214/ijraset.2021.36154

Choudhury B, Choudhury A. (2012) Dopant induced changes in structural and optical properties of Cr3+ doped TiO2 nanoparticles Materials Chemistry and Physics 132(2-3):1112-1118. https://doi.org/10.1016/j.matchemphys.2011.12.083

Choudhury B, Choudhury A (2013) Oxygen vacancy and dopant concentration dependent magnetic properties of Mn doped TiO2 nanoparticle. Curr Appl Phys 13(6):1025–1031. https://doi.org/10.1016/j.cap.2013.02.007

Cruz MRA, Sanchez-Martinez D, Torres-Martínez LM (2019) Optical properties of TiO2 thin films deposited by DC sputtering and their photocatalytic performance in photoinduced process. Int J Hydrogen Energy 44(36):20017–20028. https://doi.org/10.1016/j.ijhydene.2019.06.043

Dandia A, Saini P, Sharma R, Parewa V (2020) Visible light driven perovskite-based photocatalysts: A new candidate for green organic synthesis by photochemical protocol. Current Research in Green and Sustainable Chemistry 3:100031. https://doi.org/10.1016/j.crgsc.2020.100031

Daude N, Gout C, Jouanin C (1977) Electronic band structure of titanium dioxide. Phys Rev B 15(6):3229–3235. https://doi.org/10.1103/PhysRevB.15.3229

Deng Z, Dai Y, Chen W, Pei X, Liao J (2010) Synthesis and characterization of bowl-like single-crystalline BaTiO 3 nanoparticles. Nanoscale Res Lett 5(7):1217–1221. https://doi.org/10.1007/s11671-010-9629-7

Dong H, Zeng G, Tang L, Fan C, Zhang C, He X, and He Y. (2015) An overview on limitations of TiO2-based particles for photocatalytic degradation of organic pollutants and the corresponding countermeasures. In Water Research (Vol. 79). Elsevier Ltd. https://doi.org/10.1016/j.watres.2015.04.038

Duta M, Predoana L, Calderon-Moreno JM, Preda S, Anastasescu M, Marin A, Dascalu I, Chesler P, Hornoiu C, Zaharescu M, Osiceanu P, Gartner M (2016) Nb-doped TiO2 sol-gel films for CO sensing applications. Mater Sci Semicond Process 42:397–404. https://doi.org/10.1016/j.mssp.2015.11.004

Eleutério T, Sério S, Teodoro OMND, Bundaleski N, Vasconcelos HC (2020) XPS and FTIR studies of DC reactive magnetron sputtered TiO2 thin films on natural based-cellulose fibers. Coatings 10(3):61–71. https://doi.org/10.3390/coatings10030287

Eyssler A, Mandaliev P, Winkler A, Hug P, Safonova O, Figi R, Weidenkaff A, Ferri D (2010) The effect of the state of pd on methane combustion in Pd-Doped LaFeO 3. J Phys Chem C 114(10):4584–4594. https://doi.org/10.1021/jp911052s

Feng Y, Qi R, Jiang L, Huang Q, Li T, Liu G, Li W, Yan W, Zhang Z, Wang Z (2021) Chemical modification of B4C films and B4C/Pd layers stored in different environments. Materials 14(5):1319. https://doi.org/10.3390/ma14051319

Gade R, Ahemed J, Yanapu KL, Abate SY, Tao YT, Pola S (2018) Photodegradation of organic dyes and industrial wastewater in the presence of layer-type perovskite materials under visible light irradiation. J Environ Chem Eng 6(4):4504–4513. https://doi.org/10.1016/j.jece.2018.06.057

Gandhi AC, Wu SY (2017) Strong deep-level-emission photoluminescence in NiO nanoparticles. Nanomaterials 7(8):18–20. https://doi.org/10.3390/nano7080231

Ganesh I, Gupta AK, Kumar PP, Sekhar PS, Radha K, Padmanabham G, Sundararajan G. (2012) Preparation and characterization of Ni-doped TiO2 materials for photocurrent and photocatalytic applications. Sci World J. 2012(October 2016). https://doi.org/10.1100/2012/127326

Ge L, Xu M (2006) Influences of the Pd doping on the visible light photocatalytic activities of InVO4-TiO2 thin films. Mater Sci Eng, B 131(1–3):222–229. https://doi.org/10.1016/j.mseb.2006.04.021

Gopinath KP, Madhav NV, Krishnan A, Malolan R, Rangarajan G (2020) Present applications of titanium dioxide for the photocatalytic removal of pollutants from water: A review. J Environ Manage 270(March):110906. https://doi.org/10.1016/j.jenvman.2020.110906

Irie H, Watanabe Y, Hashimoto K (2003) Nitrogen-concentration dependence on photocatalytic activity of TiO2-xNx powders. J Phys Chem B 107(23):5483–5486. https://doi.org/10.1021/jp030133h

Ismail AA (2012) Mesoporous PdO-TiO 2 nanocomposites with enhanced photocatalytic activity. Appl Catal B 117–118:67–72. https://doi.org/10.1016/j.apcatb.2012.01.006

Jenck JF, Agterberg F, Droescher MJ (2004) Products and processes for a sustainable chemical industry: A review of achievements and prospects. Green Chem 6(11):544–556. https://doi.org/10.1039/b406854h

Kavi Rasu K, Sakthivel P, Prasanna Venkatesan GKD (2020) Effect of Pd2+ co-doping on the structural and optical properties of Mn2+:ZnS

nanoparticles. Opt Laser Technol 130(May):106365. https://doi.org/10.1016/j.optlastec.2020.106365
Kumar Patnaik R, Divya N (2023) A brief review on the synthesis of TiO2 thin films and its application in dye degradation. Materials Today: Proceedings 72:2749–2756. https://doi.org/10.1016/J.MATPR.2022.10.064
Lellis B, Fávaro-Polonio CZ, Pamphile JA, Polonio JC (2019) Effects of textile dyes on health and the environment and bioremediation potential of living organisms. Biotechnology Research and Innovation 3(2):275–290. https://doi.org/10.1016/J.BIORI.2019.09.001
Liqiang J, Yichun Q, Baiqi W, Shudan L, Baojiang J, Libin Y, Wei F, Honggang F, Jiazhong S (2006) Review of photoluminescence performance of nano-sized semiconductor materials and its relationships with photocatalytic activity. Sol Energy Mater Sol Cells 90(12):1773–1787. https://doi.org/10.1016/j.solmat.2005.11.007
Liu B, Wang X, Cai G, Wen L, Song Y, Zhao X (2009) Low temperature fabrication of V-doped TiO2 nanoparticles, structure and photocatalytic studies. J Hazard Mater 169(1–3):1112–1118. https://doi.org/10.1016/j.jhazmat.2009.04.068
Liu J, Zhang JG, Yang Z, Lemmon JP, Imhoff C, Graff GL, Li L, Hu J, Wang C, Xiao J, Xia G, Viswanathan VV, Baskaran S, Sprenkle V, Li X, Shao Y, Schwenzer B. (2013) Materials Science and Materials Chemistry for Large Scale Electrochemical Energy Storage : From Transportation to Electrical Grid. 23(8):929–946. https://doi.org/10.1002/adfm.201200690
Lu Y, Khan S, Song CL, Wang KK, Yuan GZ, Li W, Han GR, Liu Y (2016) Doping concentration effects upon column-structured Nb:TiO2 for transparent conductive thin films prepared by a sol-gel method. J Alloy Compd 663:413–418. https://doi.org/10.1016/j.jallcom.2015.12.102
Matussin SN, Khan F, Harunsani MH, Kim YM, Khan M. (2023). Effect of Pd-Doping Concentrations on the Photocatalytic Photoelectrochemical and Photoantibacterial Properties of CeO2 Catalysts 13(1):96. https://doi.org/10.3390/catal13010096
Mcbride JR, Hass KC, Weber WH, Weber WH (1991) Resonance-Raman and Lattice-Dynamics studies of single crystal PdO. Physic Rev B 44(10):5016–5028. https://doi.org/10.1103/PhysRevB.44.5016
Meetei SD, Singh SD. (2014) Effects of crystal size structure and quenching on the photoluminescence emission intensity lifetime and quantum yield of ZrO2:Eu3+ nanocrystals Journal of Luminescence 147: 328-335. https://doi.org/10.1016/j.jlumin.2013.11.064
Mekprasart W, Khumtong T, Rattanarak J, Techitdheera W, Pecharapa W (2013) Effect of nitrogen doping on optical and photocatalytic properties of TiO2 thin film prepared by spin coating process. Energy Procedia 34:746–750. https://doi.org/10.1016/j.egypro.2013.06.809
Meng F, Dai C, Liu Z, Luo S, Ge J, Duan Y, Chen G, Wei C, Chen RR, Wang J, Mandler D, Xu ZJ (2022) Methanol electro-oxidation to formate on iron-substituted lanthanum cobaltite perovskite oxides. Escience 2(1):87–94. https://doi.org/10.1016/j.esci.2022.02.001
Musić S, Filipović-Vinceković N, Sekovanić L (2011) Precipitation of amorphous SiO2 particles and their properties. Braz J Chem Eng 28(1):89–94. https://doi.org/10.1590/S0104-66322011000100011
Nandoost A, Bahramifar N, Moghadamnia AA, Kazemi S. (2022) Adsorption of Malachite Green (MG) as a Cationic Dye on Amberlyst 15, an Ion-Exchange Resin. J Environ Public Health, 2022. https://doi.org/10.1155/2022/4593835
Nath J, Singh VP, Sehgal R, Kumar S, Kumar V, Sehgal R (2023) Utilization of magnetic nanoferrite-based photocatalysts for elimination of organic pollutants from wastewater. Magnetic Nanoferrites and Their Composites: Environmental and Biomedical Applications 317–350:317. https://doi.org/10.1016/B978-0-323-96115-8.00008-8
Pal M, Pal U, Gracia JM, Perez-Rodriguez F. (2012) Effects of crystallization and dopant concentration on the emission behavior of TiO2:Eu nanophosphors, Nanoscale Research Letters 7(1). https://doi.org/10.1186/1556-276X-7-1
Pan F, Lin H, Zhai H, Miao Z, Zhang Y, Xu K, Guan B, Huang H, Zhang H (2018) Pd-doped TiO2 film sensors prepared by premixed stagnation flames for CO and NH3 gas sensing. Sens Actuators, B Chem 261:451–459. https://doi.org/10.1016/j.snb.2018.01.173
Panthi G, Park M (2022) Approaches for enhancing the photocatalytic activities of barium titanate: A review. J Energy Chem 73:160–188. https://doi.org/10.1016/J.JECHEM.2022.06.023
Passi M, Pal B (2021) A review on CaTiO3 photocatalyst: Activity enhancement methods and photocatalytic applications. Powder Technol 388:274–304. https://doi.org/10.1016/J.POWTEC.2021.04.056
Perdomo F, Figueroa R, Obtenido B, El, P. O. R., Coprecipitación M. D. E., & Perdomo, C. F. (2008). BaTiO 3 OBTENIDO POR EL MÉTODO DE COPRECIPITACIÓN BaTiO 3 OBTAINED BY COPRECIPITATION METHOD.
Portia SAU, Srinivasan R, Elaiyappillai E, Johnson PM, Ramamoorthy K (2020) Facile synthesis of Eu-doped CaTiO3 and their enhanced supercapacitive performance. Ionics 26(7):3543–3554. https://doi.org/10.1007/s11581-020-03494-9
Rahman TU, Roy H, Fariha A, Shoronika AZ, Al-Mamun MR, Islam SZ, Islam MS, Marwani HM, Islam A, Alsukaibi AKD, Rahman MM, Awual MR (2023) Progress in plasma doping semiconductor photocatalysts for efficient pollutant remediation and hydrogen generation. Sep Purif Technol 320:124141. https://doi.org/10.1016/J.SEPPUR.2023.124141
Sarma M, Jaiswal MK, Podder S, Bora J, Karmakar S, Choudhury B, Pal AR (2023) A study on the applicability of thin film over powder for visible light photocatalysis. Physica B 670:415354. https://doi.org/10.1016/J.PHYSB.2023.415354
Sathasivam S, Bhachu DS, Lu Y, Chadwick N, Althabaiti SA, Alyoubi AO, Basahel SN, Carmalt CJ, Parkin IP (2015) Tungsten doped TiO 2 with enhanced photocatalytic and optoelectrical properties via aerosol assisted chemical vapor deposition. Sci Rep 5(April):1–10. https://doi.org/10.1038/srep10952
Sharma J, Sharma S, Soni V (2023) Toxicity of malachite green on plants and its phytoremediation: A review. Regional Studies in Marine Science 62:102911. https://doi.org/10.1016/J.RSMA.2023.102911
Sohrabian M, Mahdikhah V, Alimohammadi E, Sheibani S (2023) Improved photocatalytic performance of SrTiO3 through a Z-scheme polymeric-perovskite heterojunction with g-C3N4 and plasmonic resonance of Ag mediator. Appl Surf Sci 618:156682. https://doi.org/10.1016/J.APSUSC.2023.156682
Toma FTZ, Rahman S, Rahman S, Hussain KA, Ahmed S. (2024) Thin Film Deposition Techniques: A Comprehensive Review. J Mod Nanotechnol 4:6. https://doi.org/10.53964/jmn.2024006
Wang W, Xu M, Xu X, Zhou W, Shao Z (2020) Perovskite Oxide Based Electrodes for High-Performance Photoelectrochemical Water Splitting. Angewandte Chemie - International Edition 59(1):136–152. https://doi.org/10.1002/anie.201900292
Wang R, Du L, Gao W, Li J, Tsona NT, Zhang X, Hu X, Wang W, Liu H (2021) Enhanced photocatalytic performance of PdO-loaded heterostructured nanobelts to degrade phenol. Chemosphere 276:130266. https://doi.org/10.1016/j.chemosphere.2021.130266
Won DJ, Wang CH, Jang HK, Choi DJ (2001) Effects of thermally induced anatase-to-rutile phase transition in MOCVD-grown TiO2 films on structural and optical properties. Appl Phys A Mater Sci Process 73(5):595–600. https://doi.org/10.1007/s003390100804
Wu LQ, Li YC, Li SQ, Li ZZ, Tang GD, Qi WH, Xue LC, Ge XS, Ding LL (2015) Method for estimating ionicities of oxides using O1s photoelectron spectra. AIP Adv 5(9):1–7. https://doi.org/10.1063/1.4931996
Yu Y, He T, Guo L, Yang Y, Guo L, Tang Y, Cao Y (2015) Efficient visible-light photocatalytic degradation system assisted by conventional Pd catalysis. Sci Rep 5:1–7. https://doi.org/10.1038/srep09561
Zhang H, Xing Z, Zhang Y, Li Z, Wu X, Liu C, Zhu Q, Zhou W (2015) Ni2+ and Ti3+ co-doped porous black anatase TiO2 with unprecedented-high visible-light-driven photocatalytic degradation performance. RSC Adv 5(129):107150–107157. https://doi.org/10.1039/c5ra23743b

Publisher's Note